Construction and Building Materials 164 (2018) 164–177

Contents lists available at ScienceDirect

Construction and Building Materials

journal homepage: www.elsevier.com/locate/conbuildmat

Hybrid NSE/EB technique for shear strengthening of reinforced concrete beams using FRCM: Experimental study

Tadesse G. Wakjira [a], Usama Ebead [b,*]

[a] Department of Civil and Architectural Engineering, College of Engineering, Qatar University, P.O. Box 2713, Doha, Qatar
[b] Department of Civil and Architectural Engineering, College of Engineering, Qatar University, P. O. Box 2713, Doha, Qatar

HIGHLIGHTS

- NSE/EB pioneer FRCM systems were examined for shear strengthening of RC beams.
- Thirteen beams under three-point loading have been tested.
- Carbon-FRCM showed the highest increase in the load carrying capacity of 83%.
- PBO-FRCM showed the least increase in the load carrying capacity of 62%.
- Near surface embedding of FRCM mitigate deboning.

ARTICLE INFO

Article history:
Received 30 September 2017
Received in revised form 3 December 2017
Accepted 27 December 2017
Available online 2 January 2018

Keywords:
Reinforced concrete
Fabric reinforced cementitious matrix (FRCM)
Beam
Shear
Strengthening
Near surface embedded FRCM system (NSE-FRCM)
Hybrid near surface embedded and externally bonded FRCM system (NSEEB-FRCM)

ABSTRACT

The externally bonded (EB) fabric reinforced cementitious matrix (FRCM) has successfully been used as a structural strengthening for various applications including flexural and shear strengthening of reinforced concrete (RC) beams, flexural strengthening of RC slabs and column confinement. However, the EB-FRCM system is characterized by poor FRCM/concrete bond leading to premature debonding of FRCM off the concrete substrate, particularly for thicker FRCM. The present paper reports on an experimental study on the efficacy of a pioneer form of hybrid near surface embedded and externally bonded technique using FRCM composites (NSEEB-FRCM) for shear strengthening of RC beams. With such a technique, higher thickness of FRCM composites can be applied with less likelihood of debonding that is normally experienced when using the EB-FRCM system. Thirteen shear-deficient medium-scale RC beams were constructed, strengthened in shear and tested under three-point bending test. The test parameters were: (a) FRCM type (polyparaphenylene benzobisoxazole, carbon, and glass), (b) strengthening configuration (full versus intermittent strips), and (c) number of fabric layers.

The percentage enhancement in the shear capacity of the beams ranged from 43% to 114% indicating the successful implementation of the strengthening methods provided. An average enhancement in shear capacity of 83%, 72% and 62% were observed in carbon FRCM, glass FRCM and PBO-FRCM, respectively. The failure mode of the strengthened specimens was sensitive to the type and configuration of FRCM in addition to the number of FRCM layers. The strengthening systems also resulted in higher deflection at failure and energy absorption value of the strengthened beams with an average of 94% and 204% relative to the reference specimen, respectively.

1. Introduction

Retrofitting of deteriorated or deficient structures has become one of the main concern in the construction industry. The corrosion of steel bars is a major cause of deterioration that requires a remedy through the structural strengthening. Other factors causing structural deterioration include the increase in service loads caused by change in occupancy, deficiencies in design and/or construction, severe environmental conditions like hurricane and seismic events, and the lack of proper maintenance. A considerable amount of research has been carried out for developing strengthening systems that increase the load carrying capacity and ductility of the deteriorated structures; hence, extend their life span. In recent years, the development of fabric reinforced cementitious

* Corresponding author.
E-mail addresses: twakjira@qu.edu.qa (T.G. Wakjira), uebead@qu.edu.qa (U. Ebead).

https://doi.org/10.1016/j.conbuildmat.2017.12.224
0950-0618/

matrix (FRCM) composites is receiving popularity as a viable alternative strengthening materials that overcome the problems associated with the use of fiber reinforced polymer (FRP) composites [1–3]. FRP composites are incompatible with the concrete substrate usually leading to debonding [4]. Moreover, these composites are susceptible to failure at high-temperatures and are also problematic to apply on wet surfaces [4,5]. The replacement of epoxy with cement based matrix in FRCM composites, on the other hand, reduces the chance of debonding attributed to its' compatibility with the concrete substrate. FRCM composites possess good resistance to fire and elevated temperature [6,7] and can also be applied at a temperature as low as 0 °c [3].

Existing literature revealed effective uses of FRCM techniques for the structural strengthening of a variety of applications; e.g., including column confinement [8–10], flexural strengthening of RC beams [11–14], shear strengthening of RC beams [15–19], and flexural strengthening of RC slab [20]. FRCM composites can also be used to increase the ductility of the strengthened members [18,19,21]. In some cases, the application of FRCM strengthening systems changed the brittle shear failure into ductile flexural failure due to the large increase in the shear resistance of the strengthened beams [4]. Different techniques of FRP application have been developed through time among which the externally bonded (EB) [22–25], near surface mounted (NSM) [26–33], mechanically fastened [34], hybrid externally bonded and mechanically fastened [35,36] were commonly reported. The research work on FRCM systems; however, focused mainly on the use of externally bonded FRCM systems with anchorage [17,37] or without anchorage [2,5,18,21,38,39].

The efficacy of FRCM for the strengthening of shear-deficient RC beams is influenced by various factors including the number of fabric layers or FRCM thickness [4,5,16–18,39–42], wrapping scheme [4,16,38,43], internal shear reinforcement [39], geometric configuration [19,41,44], presence of end anchorage [2,17,37,42], fabric orientation [5], and fabric type [7,40,45]. With regard to the fabric type, the majority of the research work has focused on the use of a single fabric type; namely, carbon [4,16,39,40,42,46], glass [37], PBO [2,18,19], or basalt [5]. There is very few literature available on the comparison of the efficacy among different types of FRCM techniques for shear strengthening of RC beams [45]. A comparison between two FRCM types; namely, carbon FRCM and glass FRCM, was conducted for the shear strengthening of RC beams [17,38]. A comparison was also made among the PBO, carbon, and glass FRCM techniques, for the shear strengthening of RC beams [21,45].

Increasing the number of fabric layers of FRCM results in an increase in its thickness. Strengthening with larger number of fabric layers is associated with debonding of EB-FRCM off the concrete substrate; thus, decreasing the utilization of FRCM strengthening material [16,18,47]. The NSE-FRCM strengthening system is believed to prevent or reduce the premature debonding failure. However, the NSE technique is limited to a certain number of fabric layers that can be embedded within the concrete cover. As a solution to such an issue, the authors have developed a pioneer utilization of the hybrid form of NSE and EB technique called NSEEB-FRCM as will be referred to in this paper. This new form of the NSEEB-FRCM utilized two layers of fabrics in constituting the near surface embedded FRCM part and additional two layers of fabrics for the EB-FRCM part with different FRCM configurations, resulting in a total of four layers of fabrics in the FRCM system.

In light of the aforementioned gaps, the present study; therefore, aims at introducing a new form of NSEEB-FRCM system for the shear strengthening of RC beams using three commercially available FRCM systems; namely, PBO-, carbon-, and glass-FRCM. For this purpose, experimental tests have been carried out on thirteen (13) medium-scale RC beams. To avoid long sentences in this paper, FRCM layers will refer to the number of fabrics used inside the FRCM. In addition, specimens strengthened using FRCM system will be referred to as FRCM specimens.

2. Testing program

2.1. Materials

2.1.1. Reinforced concrete

The specimens were cast using ready-mixed concrete of the same batch. The concrete mix comprised 800 kg of fine aggregate, 1100 kg of course aggregate, 371 kg of ordinary Portland cement, and 168 kg of water, for each cubic meter of concrete. The concrete characteristic compressive strength was obtained by testing standard concrete cylinders with dimensions of 150 mm in diameter and 300 mm in height according to ASTM C39/C39M [48]. The test results showed an average 28-day cylindrical compressive strength of 30 ± 1.65 MPa.

The reinforcement involved 16 mm diameter bars (used as tensile reinforcement) and 8 mm diameter bars (used as compressive reinforcement and shear link) with an average yield stress of 594 MPa and 536 MPa, respectively. Table 1 summarizes the results of the average mechanical properties of the reinforcement bars based on tested samples at the laboratory.

2.1.2. Fabric-reinforced cementitious matrix

Three commercially available fabric types were utilized in this study with their producer-recommended associated mortars to form three FRCM systems; namely, carbon (C)-FRCM [49], PBO-FRCM [50] and glass (G)-FRCM [51]. Table 2 summarizes the geometric and mechanical characteristics of each fabric type along with the corresponding mortar strength as provided by the manufacturers. Moreover, the geometry of the fabric is shown in Fig. 1a through c for carbon, glass and PBO fabrics, respectively. The center to center stitch spacing in glass fabric was 18 × 14 mm while it was 10 × 10 mm and 10 × 17 mm for carbon and PBO fabrics, respectively.

2.2. Specimens and test matrix

The construction of the test specimens involved a total of thirteen (13) medium-scale RC rectangular beams of dimensions 150 mm in width, 330 mm in depth and 2100 mm in length. Fig. 2a shows the longitudinal section of the beams. A constant value of 34 mm of concrete cover was provided, yielding a typical beam effective depth of 280 mm. The specimens were tested under three-point loading as simply supported with a clear span of 1.9 m between the supports. One specimen was un-strengthened to act as a benchmark, while the remaining twelve specimens were strengthened for shear using FRCM systems. Nine of the strengthened specimens used NSEEB-FRCM system while the other three specimens were strengthened using NSE-FRCM counterpart for the purpose of comparison. Fig. 2b and c show the cross-sectional details for the NSE-FRCM and NSEEB-FRCM strengthened specimens, respectively. The NSEEB-FRCM involved two layers of near surface embedded FRCM and two more layers of EB-FRCM with different configurations, resulting in a total of 4 layers of FRCM, while the NSE-FRCM utilized two layers of fabric applied in the prepared groove with its' associated mortar.

The experimental test matrix is provided in Table 3. The specimen designation follows two key parameters, namely; fabric type and FRCM configuration for both near surface embedded and EB-FRCM system. For NSEEB-FRCM system, the specimen designation is labelled using "A-B-D" format as shown in Table 3. "A" denotes the fabric type (C- for carbon, P- for PBO, and G- for glass); "B" and "D" denotes the strengthening configuration ("I"-represent inter-

Table 1
Steel reinforcement properties (average).

Rebar Diameter (mm)	Yield stress (MPa)	COV (%)	Yield strain ε_y (%)	COV (%)	Ultimate strain (%)	COV (%)	Elastic modulus (GPa)
8	535	0.033	0.258	0.012	12.47	0.158	207
16	595	0.035	0.266	0.018	9.12	0.194	224

Table 2
Properties of fabric and associated mortars for the FRCM systems adopted.

Fabric type	c/c spacing warp × weft (mm)	A_f-warp (mm^2/mm)	A_f-weft (mm^2/mm)	Elastic modulus (GPa)	Tensile strength (GPa)	Ultimate strain (%)	28-day compressive strength of mortar (MPa)	Tensile strength of mortar (MPa)
Carbon	10 × 10	0.047	0.047	240	4.8	1.8	20	3.5
Glass	18 × 14	0.047	0.066	80	2.6	3.25	40	8.3
PBO	10 × 17	0.0455	0.0155	270	5.8	2.15	30	4.0

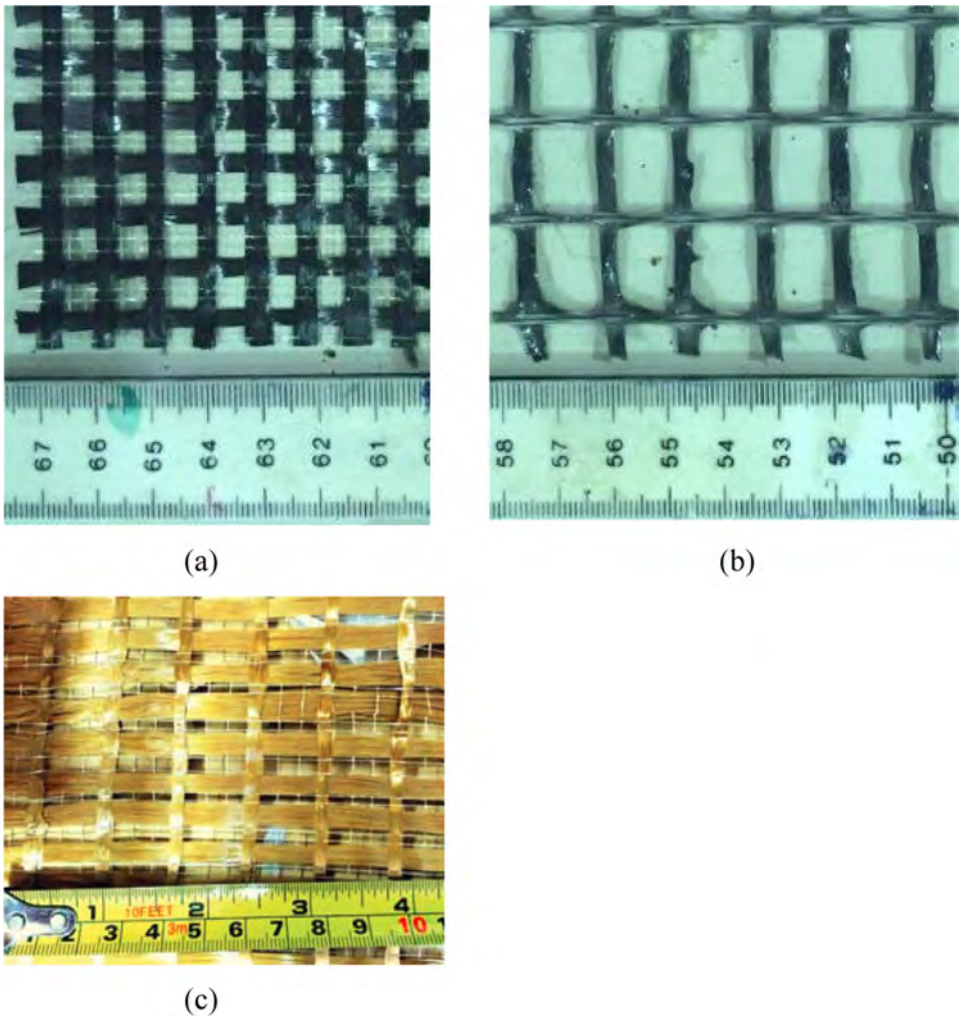

Fig. 1. Geometry of fabrics: (a) carbon fabric, (b) glass fabric and (c) PBO fabric.

mittent strips configuration, and "F"-represents full configuration) for near surface embedded and EB-FRCM system, respectively. Accordingly, C-I-I denotes a test specimen strengthened with carbon NSEEB-FRCM system in which both the near surface embedded and the externally bonded parts are intermittent as shown in Fig. 2e. In the case of NSE-FRCM system, only full configuration with two layers of FRCM system has been used. Thus, only the first two letters were used for NSE-FRCM designation; namely, "A" for the fabric type and "B" for the NSE-FRCM configuration which is full configuration. Thus, G-F denotes a test specimen strengthened with two layers of glass NSE-FRCM applied in full FRCM configuration.

The test parameters were as follows:

i. Type of FRCM system: three different FRCM systems were used; namely, PBO-FRCM, carbon-FRCM, and glass-FRCM.

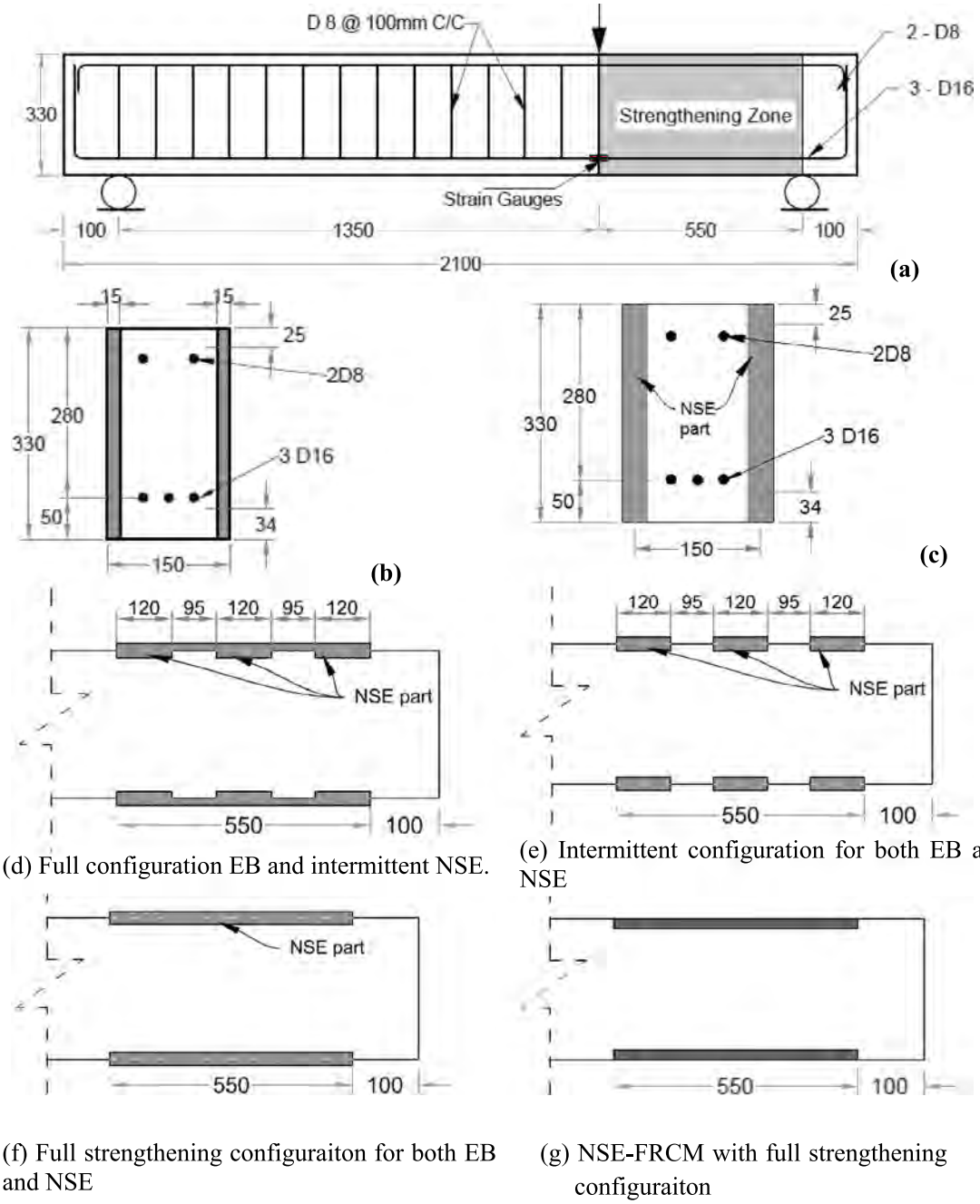

Fig. 2. Specimen details: (a) longitudinal details, (b) cross-section detail in the shear span for NSE-FRCM, (c) cross-section detail in the shear span for NSEEB-FRCM, (d) through (g) top views for all configurations.

ii. Strengthening configuration: full versus intermittent strips of NSEEB-FRCM system. The NSEEB-FRCM utilized two FRCM layers inserted in the prepared groove and two EB-FRCM layers in either full or intermittent FRCM configuration as shown in Fig. 2d through f. The intermittent FRCM configuration utilized strips of 120 mm in width and a spacing of 95 mm along the critical shear span as depicted in Fig. 2d and e. For NSE-FRCM system, only the "full" configuration of FRCM has been used as shown in Fig. 2g. The configurations were designed using preliminary calculations that assure different contributions when different spacing were provided.
iii. The effect of additional two layers of EB-FRCM system on the NSE-FRCM system.

2.3. Strengthening procedures

Fig. 3a through e summarize the preparation of the specimens and the strengthening procedure is also described herein. Firstly, grooves of 15 mm deep were created at both sides of a concrete beam using HILTI DC-SE20 slitting machine based on the FRCM configuration, as shown in Fig. 3a and b. The grooves were then sandblasted and cleaned from dust and fine particles. The concrete surface of the grooves was saturated with water for a minimum of 30 min prior to applying the FRCM to avoid water transfer from the newly applied mortar to the concrete substrate. Once the concrete surface has been saturated, a first layer of mortar was applied by means of a trowel followed by the installation of the first layer of fabric. The fabrics were installed by aligning the stronger fabric

Table 3
Test matrix.

Beam ID	Fabric type	Strengthening scheme		Number of FRCM layers	
		NSE	EB	NSE	EB
Reference	–	–	–	–	–
C-F-F	Carbon	Full/continuous	Full/continuous	2	2
C-I-F	Carbon	Intermittent	Full/continuous	2	2
C-I-I	Carbon	Intermittent	Intermittent	2	2
C-F	Carbon	Full/continuous	–	2	–
P-F-F	PBO	Full/continuous	Full/continuous	2	2
P-I-F	PBO	Intermittent	Full/continuous	2	2
P-I-I	PBO	Intermittent	Intermittent	2	2
P-F	PBO	Full/continuous	–	2	–
G-F-F	Glass	Full/continuous	Full/continuous	2	2
G-I-F	Glass	Intermittent	Full/continuous	2	2
G-I-I	Glass	Intermittent	Intermittent	2	2
G-F	Glass	Full/continuous	–	2	–

a) Cutting groove with slitting machine.

b) Removal of concrete between the grooves.

c) Installation and full impregnation of first layer of fabric (full configuration).

d) Surface finishing.

e) Finished surface (full configuration of both NSE and EB part)

Fig. 3. Strengthening preparation and procedure.

tows along the beam height. Average of 5 mm thick mortar was used between the fabric layers. Following the fiber orientation, the fabric net was embedded into the matrix with light pressure using a trowel to ensure proper impregnation of fabrics into the matrix as shown in Fig. 3c. The second layer of mortar was then applied to completely cover the fabrics. Following the same procedure, the strengthening was done until the required number of FRCM layers was obtained which was 2 and 4 layers for NSE-FRCM and NSEEB-FRCM, respectively. Finally, the surface was finished using a trowel as shown in Fig. 3d. Fig. 3e shows the finished surface that involved full configuration for both NSE and EB FRCM parts. The specimens were sealed with heissen cloth and allowed to cure for a minimum of 28 days prior to testing.

2.4. Test setup and instrumentation

The details of the test setup are depicted in Fig. 4a and b that show a beam placed in the loading frame and a view of a beam with measuring devices and gauges, respectively. Displacement-controlled loading was applied monotonically under three-point loading at a rate of 0.25 mm/min until failure using Instron 1500 HDX Static Hydraulic Universal Testing Machine. Each specimen was instrumented with two linear variable displacement transducers (LVDTs) placed directly under the loading point to monitor the displacement at each load step as shown in Fig. 4a and b. Strain gauges were used to monitor the strains in the concrete, longitudinal reinforcement and FRCM. The concrete strain gauge (60 mm length and 2% maximum strain limit) was fixed on the surface of concrete beams in the compression side just below the loading point, while other two steel strain gauges (5 mm length and 5% maximum strain limit) were installed on the tensile reinforcement bars at locations directly below the loading point. Stacked type 0°/45°/90° 3-element rosette strain gauges (30 mm gauge length and 2% maximum strain limit) were installed in the middle of all intermittent FRCM strips for obtaining the highest strain along a strip. These locations were also used in the full FRCM configuration. All strain gauge had 120 Ω resistance were installed using epoxy, CN-E, adhesive, as recommended by the manufacturer. A clip-type displacement transducer with 5 mm capacity and 100 mm gauge length was placed at the intersection between the 45-degree line extending from the loading point to the bottom of the beam and the mid-height of the cross-section to monitor the crack width as depicted in Fig. 4b. Moreover, 25 mm thick steel plate was used at the support locations in order to avoid stress concentration as shown in Fig. 4a. All data were recorded using data acquisition system at a frequency of 1 Hz.

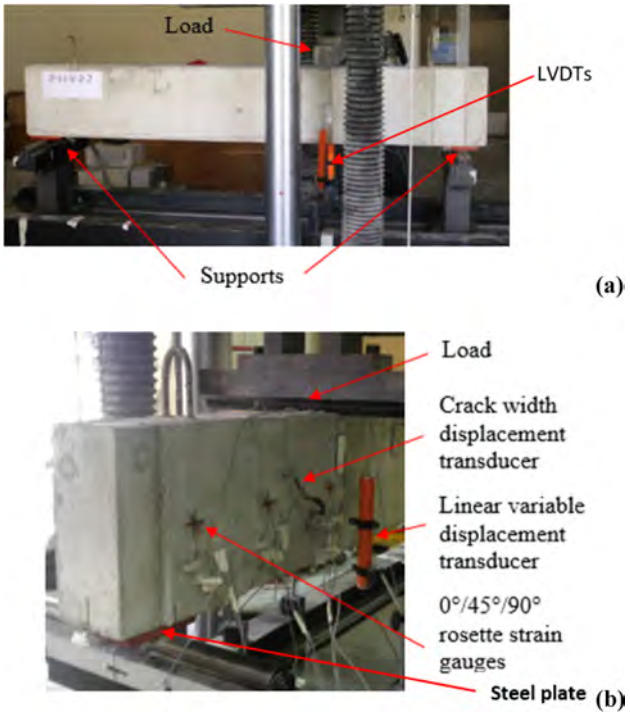

Fig. 4. Test setup: (a) specimen mounted on the loading frame; (b) a view of a specimen with measuring the measuring devices and gauges.

3. Test results and discussions

The experimental test results are summarized in Table 4 and discussed in the following sections. The comparison between the three types of FRCM composites was made based on their equivalent axial stiffness, K_f, given by Eq. (1).

$$K_f = \rho_f E_f \tag{1}$$

where E_f is the cracked modulus of elasticity of the composite and ρ_f is given by Eq. (2) below.

$$\rho_f = \frac{nA_{fv}}{d_f} \tag{2}$$

where n is the number of fabric layers in the FRCM composite, A_{fv} is the equivalent area per unit width of the fabric effective in shear and d_f is the effective depth of the fabric (280 mm). For intermittent strengthening configuration, Eq. (2) above is multiplied by a factor that represents the ratio of the shear span strengthened with the FRCM strengthening system to the total shear span length (360 mm/550 mm = 0.654).

Normalization of K_f was done with respect to K_f value for Specimen P-F. Column 3, 4 and 5 of Table 4 list the values of ρ_f, K_f and normalized K_f of strengthened specimens, respectively.

3.1. Load carrying capacity

The ultimate load carrying capacity, P_u, and the gain in the ultimate load of strengthened specimens compared to the reference specimen are summarized in Columns 2 and 3 of Table 4, respectively. The FRCM strengthening, NSE-FRCM and NSEEB-FRCM, significantly enhanced the load carrying capacity, P_u, of the specimens. The respective average overall gain in P_u for NSE-FRCM and NSEEB-FRCM specimens were 69.1% and 72.1%, which demonstrate a successful implementation of the FRCM strengthening system for shear critical RC beams.

With regard to the FRCM type, reference was made to Fig. 5a that shows the effect of the FRCM type on the shear capacity increase of the strengthened beams. C-FRCM showed higher enhancement in P_u than PBO- and G-FRCM counterparts (as shown in Fig. 5a) apparently due to higher axial stiffness of C-FRCM composite than that of the other two types of FRCM counterparts. Fig. 6 illustrates the relationship between equivalent axial stiffness of FRCM composite and the percentage of enhancement in shear capacity for specimens strengthened with NSEEB-FRCM system. From this figure, it can be observed that the gain in shear capacity is proportionality to the equivalent axial stiffness, K_f. The highest gain in P_u was recorded for specimen C-F-F (114%) corresponding to the highest K_f value as shown in Fig. 6 and Table 4. Moreover, the enhancement in P_u in the case of G-FRCM was higher than that in PBO-FRCM because glass utilizes stiffness in both the warp and weft directions almost equally. The PBO has a very small weft stiffness compared to that in the warp directions. The differences in these areas are reflected in the values of the equivalent axial stiffness, K_f, in Fig. 6 and Table 4, that shows higher for glass than that

Table 4
Experimental Test Result Summary.

1 Specimen ID	2 P_u (kN)	3 Gain in P_u (%)	4 ρ_f	5 K_f	6 Normalized K_f	7 δ_u (mm)	8 δ_u/δ_{uR}	9 $\varepsilon_{s,u}(\mu\varepsilon)$	10 $\varepsilon_{c,u}(\mu\varepsilon)$	11 Ψ (kN.mm)	12 $\varepsilon_{FRCM,U}(\mu\varepsilon)$
Reference	104.000	–	–	–	–	3.25	–	1425	–	238	–
C-F-F	222.423	113.87	0.00134	181	3.98 k	7.96	2.45	–	–	1189	–
C-I-F	205.569	97.66	0.00111	150	3.29 k	6.21	2.05	1837	1615	761	345
C-I-I	149.186	43.45	0.00088	119	2.6 k	5.45	1.68	1768	1584	485	1299
C-F	184.216	77.13	0.00067	91	1.99 k	6.48	1.99	2711	2036	753	163
P-F-F	183.307	76.26	0.00081	91	2 k	6.41	1.97	2471	1779	760	166
P-I-F	169.938	63.40	0.00067	75	1.65 k	6.30	1.94	1884	1329	653	348
P-I-I	150.480	44.69	0.00053	60	1.31 k	5.38	1.66	2203	1396	497	300
P-F	169.461	62.94	0.00041	46	k	5.93	1.82	2457	1153	632	517
G-F-F	186.828	79.64	0.00161	97	2.12 k	7.44	2.29	2565	1581	932	1840
G-I-F	185.371	78.24	0.00134	80	1.76 k	6.24	1.92	2057	1251	717	387
G-I-I	167.756	61.30	0.00106	63	1.39 k	5.71	1.76	2228	2035	600	853
G-F	173.828	67.14	0.00081	48	1.06 k	5.98	1.84	2426	1891	694	300

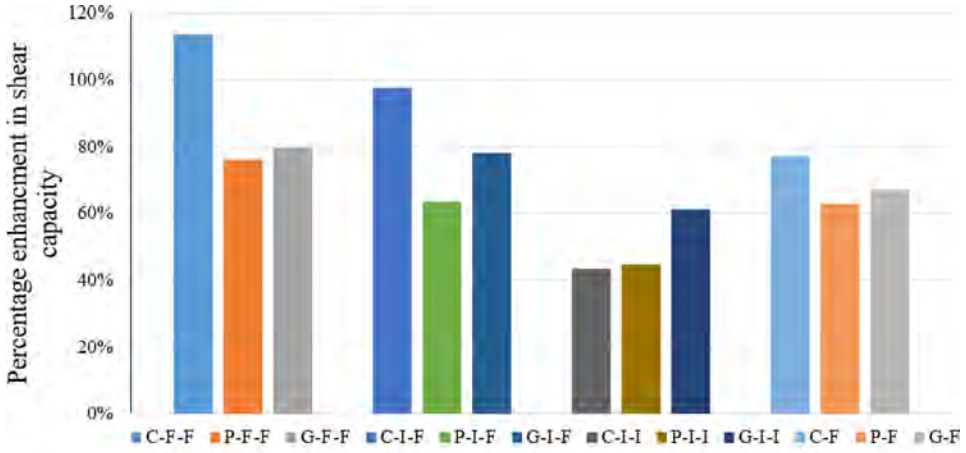

(a) Effect of FRCM type on the shear capacity increase of the strengthened beams.

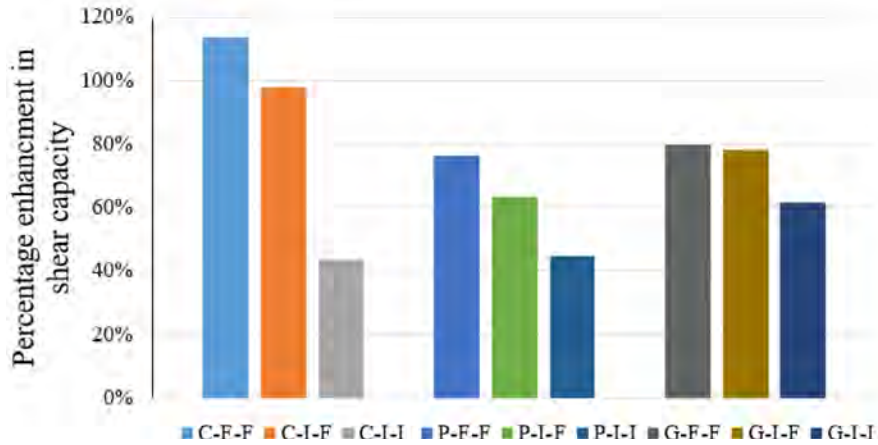

(b) Effect of the strengthening configuration on the shear capacity increase of the strenghtened beams

Fig. 5. The effect of testing parameters on the shear capacity increase of the strengthened specimens.

for PBO-FRCM. The G- and PBO-FRCM counterparts of the same configuration, G-F-F and P-F-F, show a gain in P_u of 79.6% and 76.2%, respectively as listed in Table 4.

As for the FRCM configuration, reference was made to Fig. 5b that shows the effect of the strengthening configuration on the increase in the shear capacity of the strengthened specimens. Full FRCM configuration for both NSE and EB FRCM system (Fig. 2f), showed better performance than all other FRCM configurations. Moreover, the specimens strengthened with full configuration of EB and intermittent strips of NSE (Fig. 2d) showed a significantly higher enhancement in P_u compared to the specimens strengthened with intermittent NSEEB-FRCM which involve intermittent

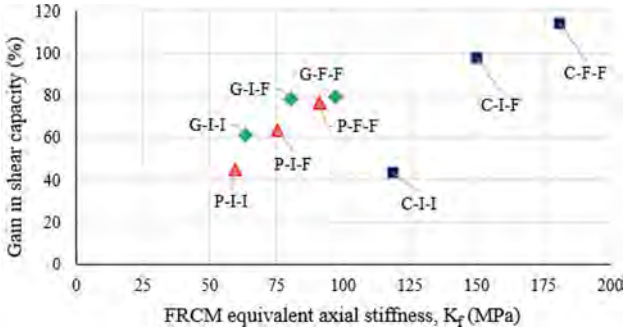

Fig. 6. Plot of equivalent axial stiffness factor versus percentage gain in shear capacity.

configuration for both NSE and EB-FRCM system (Fig. 2e). For instance, Specimen P-F-F failed at an ultimate load of 183 kN which yields 76.3% gain in shear capacity. Replacing full configuration of near surface embedded FRCM with intermittent strips (P-I-F) lowered the gain in P_u to 63.4%. Furthermore, in the specimen with intermittent strips for both NSE and EB FRCM, P-I-I, the gain in P_u was 44.7% which was 18.7% lower than the value recorded for specimen involving full FRCM configuration of EB-FRCM part and intermittent configuration of NSE-FRCM part, P-I-F as listed in Table 4. This trend was valid for both C- and G-FRCM system.

With regard to the number of FRCM layers, the addition of two layers of EB-FRCM system increased the shear capacity of the strengthened specimen compared to those of the specimens strengthened with only two layers of NSE-FRCM system of the same configuration. Specimen C-F-F, with four layers of FRCM, reached a higher load of 222 kN with respect to Specimen C-F (184 kN), owing to the contribution of the additional two layers of EB-FRCM as listed in Table 4. In PBO- and G-FRCM, specimens strengthened with four layers of FRCM, P-F-F (76.3%) and G-F-F (79.6%), showed higher gain in P_u compared with their two layers counterparts, P-F (62.9%) and G-F (67.1%). Although additional two layers of EB-FRCM increased the shear capacity, the gain in P_u was not proportional to the number of FRCM layers. This disproportionality was due to the initiation of debonding failure of the additional two layers of EB-FRCM system. Generally, no debonding failure was observed in the case of two layers of NSE-FRCM system.

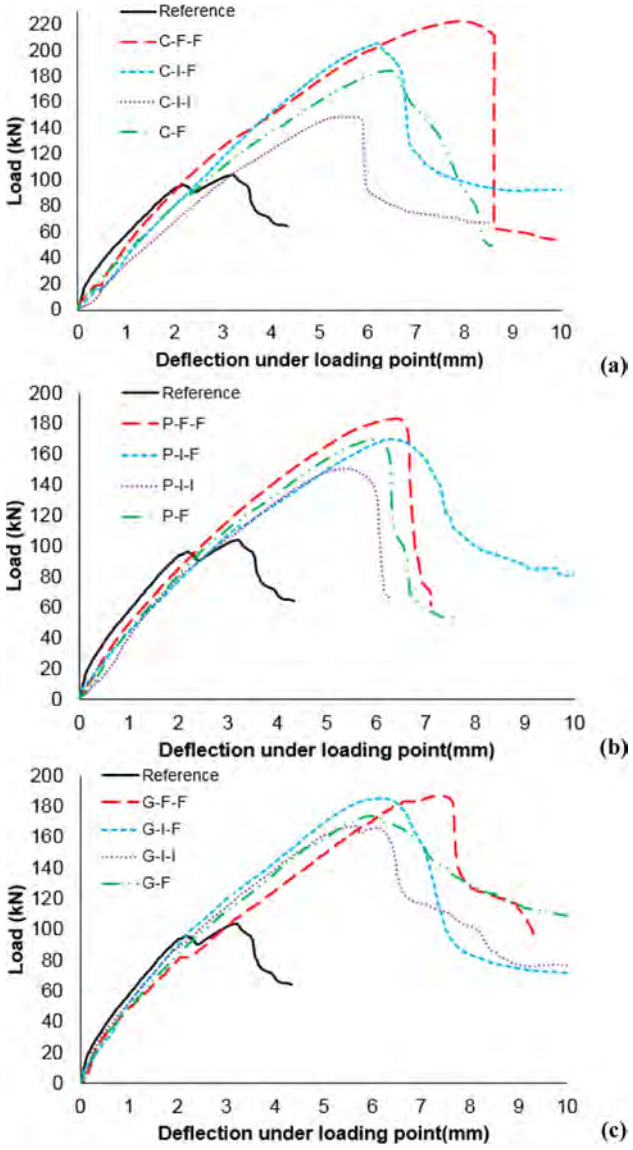

Fig. 7. Load-displacement diagrams for (a) C–FRCM strengthened specimens, (b) PBO–FRCM strengthened specimens, and (c) G–FRCM strengthened specimens.

3.2. Deformational characteristics

The load–deflection plots are depicted in Fig. 7a, b, and c for C-, PBO- and G-FRCM strengthened specimens, respectively. From these figures, it is evident that no yield zone has been observed in all specimens indicating that the steel reinforcement did not reach the yielding point. This result confirmed the shear failure in all specimens provided that the concrete in the compression zone did not crush. As shown in Fig. 7a through c, different kinds of post-peak behavior have been observed for the strengthened specimens. The specimen with full configuration of EB and intermittent strips of near surface embedded PBO-FRCM, P-I-F, as an example of the NSEEB-FRCM specimens, showed softening behavior during the post-peak zone representing traces of resistance attributed to the strengthening system.

The NSE-FRCM strengthened specimens generally exhibited a softer post-peak behavior compared to that shown by the NSEEB-FRCM counterparts. The behavior of the latter was associated with a sudden load drop due to the observed FRCM/concrete debonding. This observation indicates that additional two layers of EB-FRCM to the NSE-FRCM system reduced the ductility of the strengthened specimens due to the susceptibility of the EB component to debonding. With regard to the FRCM type, C-FRCM strengthened specimens were more ductile than the PBO-FRCM counterparts. However, no significant difference was observed in terms of the ductility behavior between C-FRCM and G-FRCM specimens.

The deflection at the ultimate load for the reference specimen (δ_{uR}) and for the strengthened specimen (δ_u) are listed in Column 7 of Table 4. Column 8 of Table 4 lists the ratio δ_u/δ_{uR} which may be considered as a measure of ductility behavior for the strengthened specimens. The strengthening system resulted in higher values of δ_u with an average of 94% relative to the reference specimen, which shows the effective implementation of FRCM shear strengthening system in improving the ductility behavior of the strengthened specimens.

With regard to the FRCM type, specimens of C-FRCM showed higher deflections at the corresponding ultimate loads than those of the G-FRCM counterparts with an exception of Specimen C-I-I. The latter showed lower δ_u value than that of the Specimen G-I-I which is due to the debonding failure observed in Specimen C-I-I. On the other hand, G-FRCM has generally showed higher δ_u value

than that of the PBO-FRCM with an exception of G-I-F. For instance, the deflection at the ultimate load was higher for Specimen C-F-F (7.96 mm) than that for Specimen G-F-F (7.44 mm) which was in turn higher than that for Specimen P-F-F (6.41 mm) as listed in Table 4.

As far as the FRCM configuration is concerned, reference was made to Fig. 2d through g. Full configuration for both NSE and EB-FRCM, as in Fig. 2f, showed higher value of δ_u than those involving intermittent configuration for NSE part and full configuration for EB-FRCM part (Fig. 2d). Furthermore, the specimens with intermittent configuration for NSE part and full configuration for EB-FRCM part (Fig. 2d) showed higher value of δ_u than those with the intermittent configuration for both NSE and EB-FRCM system (Fig. 2e). For instance, the specimen with full configuration for carbon NSEEB-FRCM, Specimen C-F-F (7.96 mm) showed higher deflection at P_u than Specimen C-I-F (6.65 mm) which was in turn higher than that for Specimen C-I-I (5.45 mm) as given in Table 4.

With regard to the strain results, Column 9 and Column 10 of Table 4 list the strain values at the ultimate load for tensile reinforcement ($\varepsilon_{s,u}$) and concrete ($\varepsilon_{c,u}$), respectively. Generally in all cases, the longitudinal steel did not yield ($\varepsilon_{s,u} < 2660\mu\varepsilon$) and the concrete in compression zone did not crush ($\varepsilon_{c,u} < 3500\mu\varepsilon$) suggesting shear failure for the beams. The strain developed in longitudinal steel has been increased for the strengthened specimens in comparison to that of the benchmark specimen with an average increase of 54.8% as given in Table 4.

Fig. 8a, b and c show the effect of the FRCM configuration and number of FRCM layers on the load versus flexural strain plot for C-, PBO-, and G-FRCM system, respectively. The specimen with full NSEEB-FRCM configuration generally showed higher values of $\varepsilon_{s,u}$ than those involving intermittent configuration. For instance, the value of $\varepsilon_{s,u}$ was higher for Specimen G-F-F (2565 με) than that for Specimens G-I-F (2057 με) and G-I-I (2228 με) (as can be seen in Table 4 and Fig. 8c). This observation indicates the significance of the number of the FRCM layers in increasing the strain in the flexural steel bar thereby enhancing the ductility of the strengthened specimen.

3.3. Energy absorption

The energy absorption (Ψ) is the integration of the load–deflection (the area under the curve) up to the peak load [52]. The energy absorption values have been significantly enhanced due to strengthening as can be seen in Column 11 of Table 4. The maximum increase in the energy absorption was reported for Specimen C-F-F (1189 kN.mm), which was about 5 times that of the benchmark specimen (Ψ_R = 238 kN.mm).

Fig. 9 shows the relationship between equivalent axial stiffness of FRCM composite and energy absorption of NSEEB-FRCM strengthened specimens. It can be seen from this figure that the energy absorption and equivalent axial stiffness has direct relationship. The C–FRCM systems, with higher axial stiffness than other FRCM composites, generally exhibited a better improvement in Ψ in comparison to that of G-FRCM counterparts which was in turn better than the PBO-FRCM. For instance, Ψ was higher for Specimen C-F-F (1189 kN.mm) than that for Specimen G-F-F (932 kN.mm) which was in turn higher than that for Specimen P-F-F (760 kN.mm) as shown in Fig. 9 and Table 4. With regard to the number of FRCM layers, the specimens with additional two layers of EB-FRCM system significantly increased the energy absorption values compared to those with only two layers of NSE-FRCM. Specimens C-F, G-F and P-F showed respective values of 753 kN.mm, 694 kN.mm, and 632 kN.mm which were lower than those with four layers of NSEEB-FRCM system counterparts (as can be seen in Fig. 9 and Table 4).

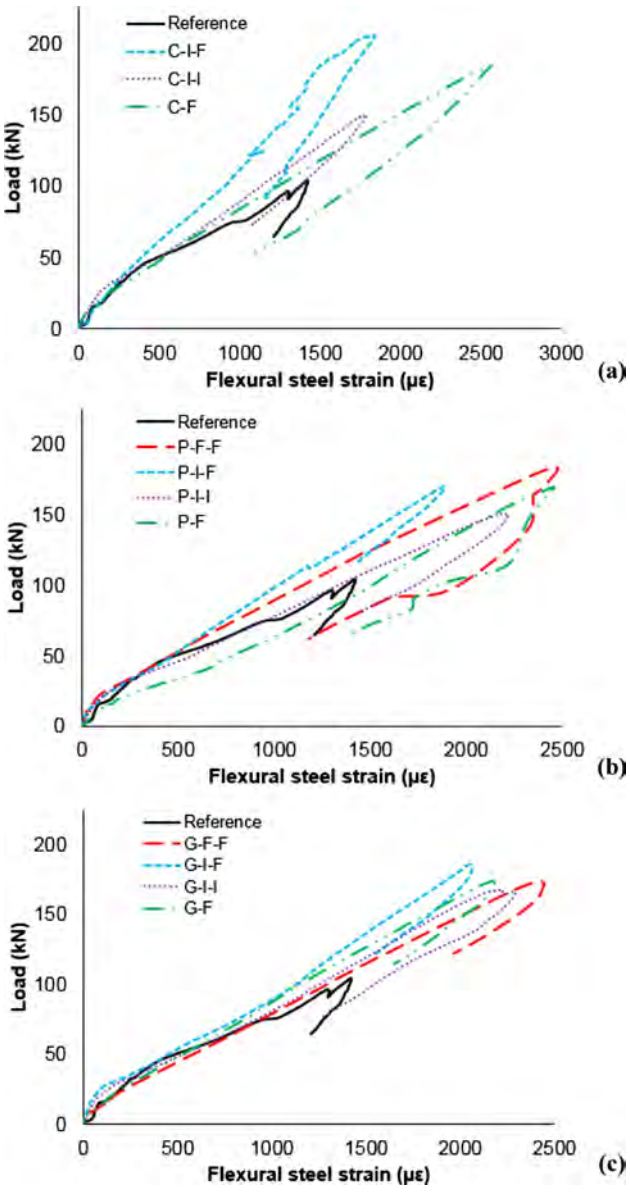

Fig. 8. Load–flexural strain diagrams for (a) C–FRCM strengthened specimens, (b) PBO–FRCM strengthened specimens, and (c) G–FRCM strengthened specimens.

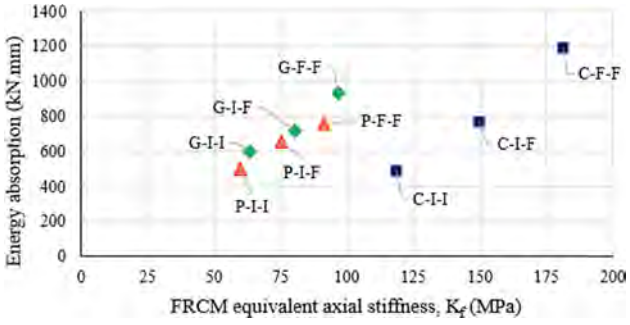

Fig. 9. Plot of equivalent axial stiffness factor versus energy absorption.

With regard to the FRCM configuration, the strengthening involving full configuration of FRCM showed better performance than that involving the intermittent counterpart. For instance, for Specimen P-F-F (760 kN.mm) changing the configuration of NSE-

FRCM from full strip (P-F-F) to intermittent strips (P-I-F) lowered the energy absorption value to 653 kN.mm. Moreover, replacing the full EB-FRCM of Specimen P-F-F with intermittent strips of Specimen P-I-I further reduced the value of Ψ to 497 kN.mm as listed in Table 4.

3.4. Crack pattern and failure modes

The crack patterns and failure modes of the strengthened specimens are illustrated in Fig. 10a through m. The reference specimen failed by typical diagonal shear failure as shown in Fig. 10a.

The major failure modes observed for the strengthened specimens are summarized below.

i. Diagonal shear crack: Major diagonal shear cracks have been observed on the surface of the FRCM for all specimens strengthened with intermittent configuration for near surface embedded FRCM and either full or intermittent configuration for EB-FRCM system as shown in Fig. 10b through g. However, the specimens strengthened with full configuration of NSEEB-FRCM system did not show a major crack on the surface of the FRCM as shown in Fig. 10h, i and j for C-F-F, P-F-F, and G-F-F, respectively. Following the completion of the test, the FRCM material was removed to expose the concrete surface to look at the actual crack patterns of the specimens. In fact, after exposing the FRCM layers, it was found that there was always a major diagonal shear crack

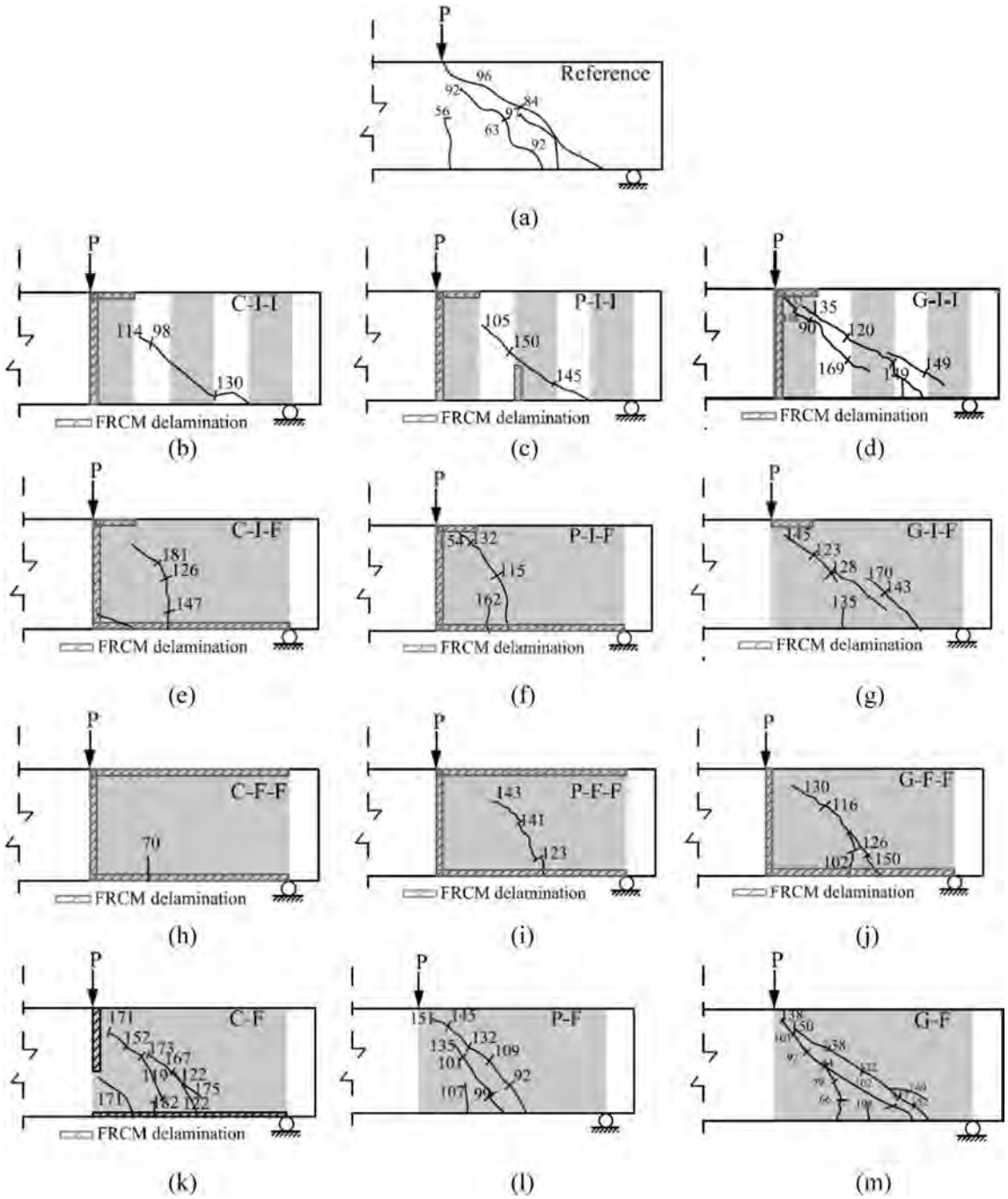

Fig. 10. Crack patterns (all values in kN) (a) reference beam, (b) C-I-I, (c) P-I-I, (c) G-I-I, (d) C-I-F, (e) P-I-F, (f) G-I-F, (g) C-F-F, (h) P-F-F, (i) G-F-F, (k) C-F, (l) P-F and (m) G-F.

on the concrete surface for all specimens as shown in Fig. 11a and b for Specimen P-F-F before and after removal of the FRCM composite, respectively.

ii. Delamination within the FRCM: In all the specimens strengthened with intermittent configuration for both NSE and EB-FRCM system, delamination of FRCM at the interface between the near surface embedded and EB-FRCM has been observed (Fig. 10b through d). The delamination of the EB-FRCM part from the NSE-FRCM part was observed only for the first strip located directly under the loading point as shown in Fig. 10b through d for Specimens C-I-I, P-I-I and G-I-I, respectively. The delamination of EB-FRCM part is due to the enhanced bond between the concrete substrate and NSE-FRCM part embedded in unlike the EB-FRCM as shown in Fig. 11c and d for Specimen G-I-I.

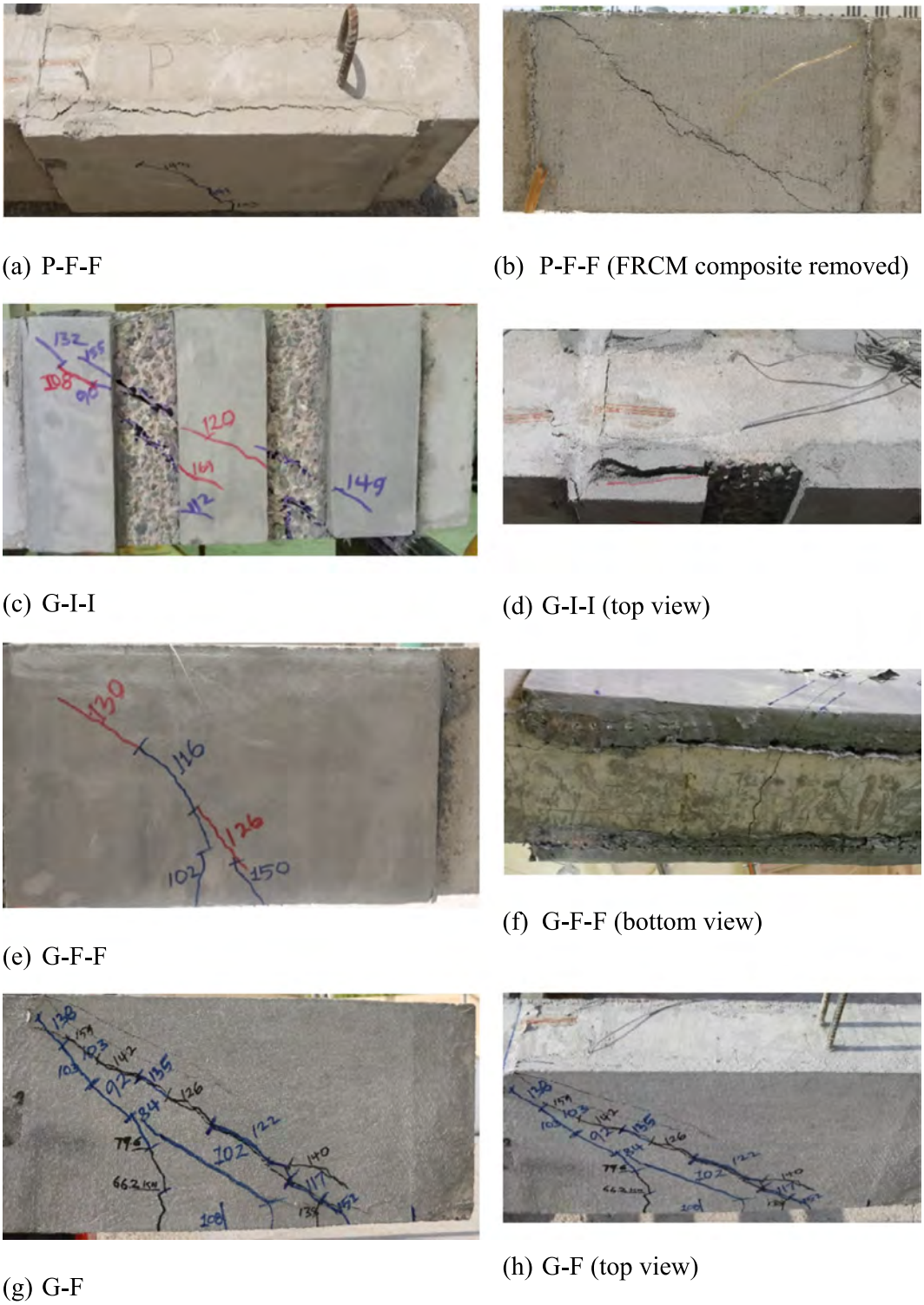

Fig. 11. Modes of failure.

iii. FRCM debonding at the interface between the concrete substrate and the FRCM system: All specimens strengthened with NSEEB-FRCM involving full configuration of EB-FRCM system failed due to the debonding of FRCM off the concrete substrate.

Case-1: In the specimens strengthened with full NSEEB-FRCM, for both NSE and EB-FRCM schemes, longitudinal debonding of the FRCM at locations near the bottom and top of the beam has been observed with an exception of specimen G-F-F (as can be seen in Fig. 10 h through j). For instance, a clear debonding of FRCM off the concrete substrate was observed on top of the beam for Specimen P-F-F as shown in Fig. 11a. In Specimen G-F-F, there was not any sign of debonding near the top of the beam; however, there was a clear debonding near the bottom surface of the beam as shown in Fig. 10j in addition to Fig. 11e and f.

Case-2: Specimens strengthened with intermittent configuration for NSE scheme and full configuration for EB-FRCM scheme showed vertical debonding of the first strip directly under the loading point along beam depth and longitudinal debonding of the FRCM near the bottom of the beam with an exception of specimen G-I-F as shown in Fig. 10e through g. In Specimen G-I-F, FRCM, debonding was observed only near the top of the beam for the first strip directly under the loading point as shown in Fig. 10g.

iv. Fabric rupture: In all the specimens strengthened with two layers of NSE-FRCM system, the failure was generally characterized by fabric rupture without any signs of debonding with an exception of C-F that failed due to the major crack developed at the FRCM and concrete interface near the bottom of the beam as shown in Fig. 10k through m. For instance, there was not any sign of debonding observed in Specimen G-F as shown in Fig. 11g and h. This result revealed that NSE-FRCM system could be used to reduce or prevent debonding failure, usually observed in the conventional externally bonded FRCM system, by enhancing the FRCM/concrete bond. This enhancement in FRCM/concrete bond is due to the fact that the FRCM attachment provided in three side of the groove. Adding of two layers of EB-FRCM on top of the NSE-FRCM system altered the failure mode from fabric rupture to debonding of FRCM off the concrete substrate.

Generally, with an exception of full FRCM configuration with NSE-FRCM part, no FRCM/concrete debonding was observed. This observation illustrates that NSEEB-FRCM system and NSE-FRCM system have reduced the debonding of FRCM off the concrete substrate due to improved FRCM/concrete bond. This improvement in FRCM/concrete bond was attributed to the attachment of FRCM composite in the prepared groove from three sides of the groove.

The failure modes have been shown to depend on the type of fabric in addition to the FRCM configuration. G-FRCM showed better concrete/FRCM bond characteristics, resulting in higher shear capacities compared to those of the PBO-FRCM counterparts.

3.5. Crack width analysis

The NSEEB-FRCM strengthening has noticeably reduced the crack widths of the strengthened specimens relative to those of the benchmark as can be seen in Fig. 12a and b that show the plots of the load–crack width for representative specimens. For instance, the reference specimen had a crack width of 0.809 mm at the ultimate load ($P_u = 104.0$kN). At the same load (104.0 kN), the crack width measured for Specimens G-F-F, G-I-I, P-I-I, and C-I-I were

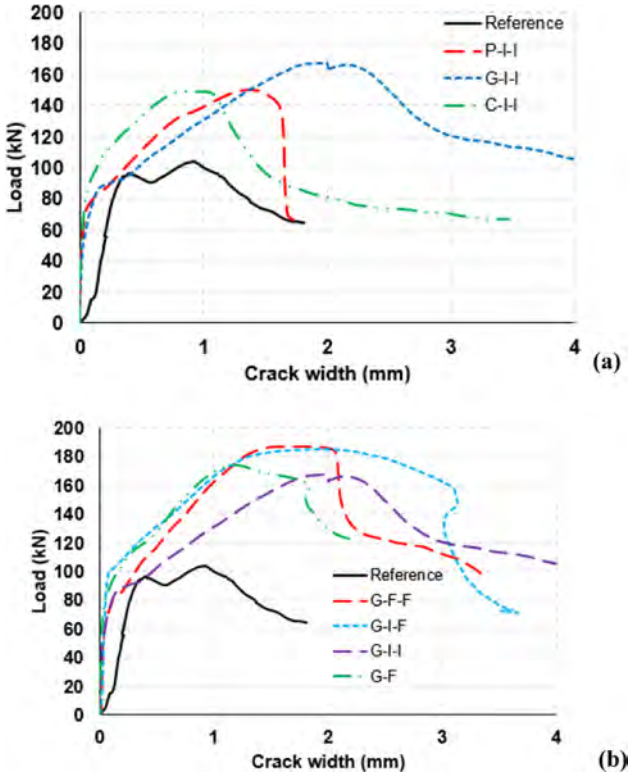

Fig. 12. Plots of crack width vs. applied load for (a) specimens strengthened with different FRCM types of intermittent NSE and intermittent EB configurations, (b) G–FRCM strengthened specimens.

0.346 mm, 0.527 mm, 0.411 mm, and 0.158 mm, respectively as shown in Fig. 12a and b.

With regard to FRCM type, the specimens strengthened with C-FRCM exhibited lower crack width values than those for PBO- and G-FRCM counterparts owing to the closely spaced fabric strands in the case of carbon FRCM as shown in Fig. 12a. Fig. 12b shows the effect of FRCM configuration on the load–crack width profiles. Full configuration for both NSE and EB-FRCM system (Fig. 2f) showed lower crack width value than those for intermittent NSE and full EB-FRCM system. Moreover, the specimens with the intermittent configuration of NSE and full configuration of EB-FRCM (Fig. 2d) showed lower crack width values than the intermittent configuration for both NSE and EB-FRCM systems (Fig. 2e). For instance, the crack width at the ultimate load for Specimen G-F-F (1.840 mm) was lower than that for Specimens G-I-F (1.971 mm) and G-I-I (2.000 mm).

3.6. Strain in FRCM system

Generally, the strain gauge located in the middle of the shear span exhibited the maximum FRCM strain. The maximum FRCM tensile strain values, $\varepsilon_{FRCM,u}$, are listed in Column 12 of Table 4. The $\varepsilon_{FRCM,u}$ values were very low as the major shear crack did not intersect with the strain gauge locations. For NSEEB-FRCM strengthening system, G-FRCM strengthened specimens showed higher FRCM strain values compared to those of the PBO-FRCM counterparts attributed to better FRCM/concrete bond in the former as listed in Table 4. For instance, the strain in Specimens G-F-F (1840$\mu\varepsilon$), G-I-F (387 $\mu\varepsilon$), and G-I-I (853 $\mu\varepsilon$) were higher than those for PBO-FRCM counterparts; namely, P-F-F (166 $\mu\varepsilon$), P-I-F (348 $\mu\varepsilon$) and P-I-I (300 $\mu\varepsilon$), respectively.

4. Conclusion

The following conclusions have been drawn on the basis of the experimental results.

- The NSEEB-FRCM strengthening system has substantially improved the shear capacity of the strengthened specimens. The enhancement in the ultimate load of up to 114% relative to the reference specimen has been achieved. Equivalent axial stiffness factor was used to compare the efficacy of the three FRCM composites. The maximum enhancement in the load carrying capacity corresponds to the highest axial stiffness. C-FRCM has generally performed better than PBO- and G-FRCM counterparts. Moreover, G-FRCM has shown to be more effective than PBO-FRCM apparently due to the higher axial stiffness in the former case. The average enhancement in P_u for C-FRCM specimens was 83.0% while it was 61.8% and 71.6% for PBO- and G-FRCM, respectively. Regarding the NSEEB-FRCM strengthening configurations, the full strengthening configuration has shown to be more effective than those involving intermittent configuration. With regard to the number of FRCM layers, provision of additional two layers of EB-FRCM system increased the ultimate load carrying capacity of the strengthened specimen relative to those using only the two layers of NSE-FRCM system. However, the increase in the shear capacity was not proportional to the number of FRCM layers. This disproportionality was caused by debonding of FRCM initiated by the additional two layers of EB-FRCM system.
- The FRCM strengthening system has generally improved the deformational characteristics of the strengthened specimens. Specimens strengthened with C-FRCM generally showed better ductile behavior than that of the PBO- and G-FRCM counterparts. In addition, G-FRCM strengthened specimens were more ductile than the PBO-FRCM counterparts. C-, G- and PBO-FRCM strengthening system resulted in higher deflection at failure with an average of 101%, 95.0% and 85.0% relative to the reference specimen, respectively. The strengthening system has also improved the energy absorption and the strains in the flexural bars of the strengthened specimens relative to the benchmark specimen. The average increase in energy absorption was 235%, 209% and 167% of that of the reference beam for C-, G, and PBO-FRCM strengthened specimens, respectively. The energy absorption of the strengthened specimen was found to have a direct relationship with equivalent axial stiffness of the FRCM composite.
- The failures in the NSEEB-FRCM strengthened specimens were characterized by delamination of the FRCM within the FRCM system (for intermittent configuration for both NSE-FRCM and EB-FRCM part) and debonding of FCRCM system at the interface between the concrete and the matrix (for full configuration of EB-FRCM part and either intermittent or full configuration for NSE-FRCM part). Generally, no debonding of FRCM was observed for NSE-FRCM strengthening system.

Acknowledgement

This paper was made possible by NPRP grant # NPRP 7-1720-2-641 from the Qatar National Research Fund (a member of Qatar Foundation). The findings achieved herein are solely the responsibility of the authors.

References

[1] U. Ebead, K.C. Shrestha, M.S. Afzal, Refai A El, A. Nanni, Effectiveness of fabric-reinforced cementitious matrix in strengthening reinforced concrete beams, J. Compos. Constr. 21 (2017) 4016084, https://doi.org/10.1061/(ASCE)CC.1943-5614.0000741.
[2] T. Trapko, D. Urbańska, M. Kamiński, Shear strengthening of reinforced concrete beams with PBO-FRCM composites, Compos. Part B 80 (2015) 63–72, https://doi.org/10.1016/j.compositesb.2015.05.024.
[3] B. Täljsten, T. Blanksvärd, Mineral-based bonding of carbon FRP to strengthen concrete structures, J. Compos. Constr. 11 (2007) 120–128, https://doi.org/10.1061/(ASCE)1090-0268(2007) 11:2(120).
[4] T.C. Triantafillou, C.G. Papanicolaou, Shear strengthening of reinforced concrete members with textile reinforced mortar (TRM) jackets, Mater. Struct. Constr. 39 (2006) 93–103, https://doi.org/10.1617/s11527-005-9034-3.
[5] Y.A. Al-Salloum, H.M. Elsanadedy, S.H. Alsayed, R.A. Iqbal, Experimental and numerical study for the shear strengthening of reinforced concrete beams using textile-reinforced mortar, J. Compos. Constr. 16 (2012) 74–90.
[6] S.M. Raoof, D.A. Bournas, TRM versus FRP in flexural strengthening of RC beams: behaviour at high temperatures, Constr. Build. Mater. 154 (2017) 424–437.
[7] Z.C. Tetta, D.A. Bournas, TRM vs FRP jacketing in shear strengthening of concrete members subjected to high temperatures, Compos. Part B 106 (2016) 190–205, https://doi.org/10.1016/j.compositesb.2016.09.026.
[8] M. Di Ludovico, A. Prota, G. Manfredi, Structural Upgrade Using Basalt Fibers for Concrete Confinement, J. Compos. Constr. (2010) 14. doi:10.1061/(ASCE)CC.1943-5614.0000114.
[9] A. Peled, Confinement of damaged and nondamaged structural concrete with FRP and TRC sleeves, J. Compos. Constr. 11 (2007) 514–522.
[10] T.C. Triantafillou, C.G. Papanicolaou, P. Zissimopoulos, T. Laourdekis, Concrete confinement with textile-reinforced mortar jackets, ACI Struct. J. 103 (2006) 28–37.
[11] T. Dantino, L.H. Sneed, C. Carloni, C. Pellegrino, Effect of the inherent eccentricity in single-lap direct-shear tests of PBO FRCM-concrete joints, Compos. Struct. (2016) 142, https://doi.org/10.1016/j.compstruct.2016.01.076.
[12] C. Escrig, L. Gil, E. Bernat-maso, Experimental comparison of reinforced concrete beams strengthened against bending with different types of cementitious-matrix composite materials, Constr. Build. Mater. 137 (2017) 317–329, https://doi.org/10.1016/j.conbuildmat.2017.01.106.
[13] A. D'Ambrisi, L. Feo, F. Focacci, Bond-slip relations for PBO-FRCM materials externally bonded to concrete, Compos. Part B Eng. 43 (2012) 2938–2949, https://doi.org/10.1016/j.compositesb.2012.06.002.
[14] S.M. Raoof, L.N. Koutas, D.A. Bournas, Textile-reinforced mortar (TRM) versus fibre-reinforced polymers (FRP) in flexural strengthening of RC beams, Constr. Build. Mater. 151 (2017) 279–291, https://doi.org/10.1016/j.conbuildmat.2017.05.023.
[15] A. Younis, U. Ebead, K. Shrestha, Tensile characterization of textile reinforced mortar, ISEC 2017 - 9th Int Struct Eng Constr Conf Resilient Struct Sustain Constr, 2017, pp. 1–6.
[16] Z.C. Tetta, L.N. Koutas, D.A. Bournas, Textile-reinforced mortar (TRM) versus fiber-reinforced polymers (FRP) in shear strengthening of concrete beams, Compos. Part B Eng. 77 (2015) 338–348, https://doi.org/10.1016/j.compositesb.2015.03.055.
[17] Z.C. Tetta, L.N. Koutas, D.A. Bournas, Shear strengthening of full-scale RC T-beams using textile-reinforced mortar and textile-based anchors, Compos. Part B Eng. 95 (2016) 225–239, https://doi.org/10.1016/j.compositesb.2016.03.076.
[18] G. Loreto, S. Babaeidarabad, L. Leardini, A. Nanni, RC beams shear-strengthened with fabric-reinforced-cementitious-matrix (FRCM) composite, Int. J. Adv. Struct. Eng. 7 (2015) 341–352, https://doi.org/10.1007/s40091-015-0102-9.
[19] L. Ombres, Structural performances of reinforced concrete beams strengthened in shear with a cement based fiber composite material, Compos. Struct. 122 (2015) 316–329.
[20] L.N. Koutas, D.A. Bournas, Flexural strengthening of two-way RC slabs with textile-reinforced mortar: experimental investigation and design equations 21 (2017) 1–11, https://doi.org/10.1061/(ASCE)CC.1943-5614.
[21] C. Escrig, L. Gil, E. Bernat-Maso, F. Puigvert, Experimental and analytical study of reinforced concrete beams shear strengthened with different types of textile-reinforced mortar, Constr. Build. Mater. 83 (2015) 248–260.
[22] A.K. Panigrahi, K.C. Biswal, M.R. Barik, Strengthening of shear deficient RC T-beams with externally bonded GFRP sheets, Constr. Build. Mater. 57 (2014) 81–91, https://doi.org/10.1016/j.conbuildmat.2014.01.076.
[23] T. El-Maaddawy, Y. Chekfeh, Shear strengthening of t-beams with corroded stirrups using composites, ACI Struct. J. 110 (2013) 779–789.
[24] T. El-Maaddawy, Y. Chekfeh, Retrofitting of severely shear-damaged concrete t-beams using externally bonded composites and mechanical end anchorage, J. Compos. Constr. 16 (2012) 693–704, https://doi.org/10.1061/(ASCE)CC.1943-5614.0000299.
[25] Q. Wang, Z. Guan, CFRP sheets for flexural strengthening of RC beams composites: part B, Compos. Part B 44 (2011) 604–612, https://doi.org/10.1016/j.compositesb.2012.02.018.
[26] F. Al-Mahmoud, A. Castel, Trinh Quang Minh, Francois R. Reinforced concrete beams strengthened with NSM CFRP rods in shear, Adv. Struct. Eng. 18 (2015) 1563–1574.
[27] S.J.E. Dias, J.A.O. Barros, NSM shear strengthening technique with CFRP laminates applied in high-strength concrete beams with or without pre-cracking, Compos. Part B Eng. 43 (2012) 290–301, https://doi.org/10.1016/j.compositesb.2011.09.006.

[28] A. Rizzo, L. De Lorenzis, Behavior and capacity of RC beams strengthened in shear with NSM FRP reinforcement, Constr. Build. Mater. 23 (2009) 1555–1567, https://doi.org/10.1016/j.conbuildmat.2007.08.014.
[29] Lorenzis L De, J.G. Teng, Near-surface mounted FRP reinforcement: an emerging technique for strengthening structures, Compos. Part B 38 (2007) 119–143, https://doi.org/10.1016/j.compositesb.2006.08.003.
[30] J.A.O. Barros, S.J.E. Dias, Near surface mounted CFRP laminates for shear strengthening of concrete beams, Cem. Concr. Compos. 28 (2006) 276–292, https://doi.org/10.1016/j.cemconcomp.2005.11.003.
[31] A. Nanni, Lorenzis L De, A. Nanni, Shear strengthening of reinforced concrete beams with near-surface mounted fiber-reinforced polymer rods, ACI Struct. J. 98 (2001).
[32] T.H. Almusallam, H.M. Elsanadedy, Y.A. Al-Salloum, S.H. Alsayed, Experimental and numerical investigation for the flexural strengthening of RC beams using near-surface mounted steel or GFRP bars, Constr. Build. Mater. 40 (2013) 145–161, https://doi.org/10.1016/j.conbuildmat.2012.09.107.
[33] I.A. Sharaky, L. Torres, J. Comas, C. Barris, Flexural response of reinforced concrete (RC) beams strengthened with near surface mounted (NSM) fibre reinforced polymer (FRP) bars, Compos. Struct. 109 (2014) 8–22, https://doi.org/10.1016/j.compstruct.2013.10.051.
[34] W.E. Elsayed, U. Ebead, K.W. Neale, Studies on mechanically fastened fiber-reinforced polymer strengthening systems, ACI Struct. J. 106 (2009) 49–59.
[35] U. Ebead, H. Saeed, Hybrid shear strengthening system for reinforced concrete beams: an experimental study, Eng. Struct. 49 (2013) 421–433, https://doi.org/10.1016/j.engstruct.2012.11.039.
[36] U. Ebead, Hybrid externally bonded / mechanically fastened fiber-reinforced polymer for RC beam strengthening, ACI Struct. J. 108 (2012) 669–678.
[37] A. Brückner, R. Ortlepp, M. Curbach, Anchoring of shear strengthening for T-beams made of textile reinforced concrete (TRC), Mater. Struct. 41 (2008) 407–418, https://doi.org/10.1617/s11527-007-9254-9.
[38] R. Azam, K. Soudki, FRCM Strengthening of shear-critical RC beams, J. Compos. Constr. 18 (2014) 4014012, https://doi.org/10.1061/(ASCE)CC.1943-5614.0000464.
[39] A. Oluwafunmilayo, T. El-Maaddawy, E.R. Ahmed, Numerical simulation and experimental testing of concrete beams strengthened in shear with fabric-reinforced cementitious matrix, J. Compos. Constr. 20 (2016) 4016056, https://doi.org/10.1061/(ASCE)CC.1943-5614.0000711.
[40] T. Blanksvärd, B. Täljsten, A. Carolin, Shear strengthening of concrete structures with the use of mineral-based composites, J. Compos. Constr. 13 (2009) 25–34, https://doi.org/10.1061/(ASCE)1090-0268(2009) 13:1(25).
[41] R. Contamine, A. Si Larbi, P. Hamelin, Identifying the contributing mechanisms of textile reinforced concrete (TRC) in the case of shear repairing damaged and reinforced concrete beams, Eng. Struct. 46 (2013) 447–458, https://doi.org/10.1016/j.engstruct.2012.07.024.
[42] E. Tzoura, T.C. Triantafillou, Shear strengthening of reinforced concrete T-beams under cyclic loading with TRM or FRP jackets, Mater. Struct. 49 (2016) 17–28.
[43] A. Si Larbi, R. Contamine, E. Ferrier, P. Hamelin, Shear strengthening of RC beams with textile reinforced concrete (TRC) plate, Constr. Build. Mater. 24 (2010) 1928–1936.
[44] J.H. Gonzalez-libreros, C. Sabau, L.H. Sneed, C. Pellegrino, G. Sas, State of research on shear strengthening of RC beams with FRCM composites, Constr. Build. Mater. 149 (2017) 444–458, https://doi.org/10.1016/j.conbuildmat.2017.05.128.
[45] A. Younis, U. Ebead, K.C. Shrestha, Different FRCM systems for shear-strengthening of reinforced concrete beams, Constr. Build. Mater. 153 (2017) 514–526, https://doi.org/10.1016/j.conbuildmat.2017.07.132.
[46] R. Azam, K. Soudki, J.S. West, M. Noël, Strengthening of shear-critical RC beams: alternatives to externally bonded CFRP sheets, Constr. Build. Mater. 151 (2017) 494–503, https://doi.org/10.1016/j.conbuildmat.2017.06.106.
[47] A. Oluwafunmilayo, T. El-Maaddawy, N. Ismail, Fabric-reinforced cementitious matrix: a promising strengthening technique for concrete structures, Constr. Build. Mater. 132 (2017) 94–111, https://doi.org/10.1016/j.conbuildmat.2016.11.125.
[48] ASTM International ASTM C39/C39M-16b, Standard Test Method for Compressive Strength of Cylindrical Concrete Specimens, ASTM International, West Conshohocken, PA, 2016. 2009:1–7.
[49] Ruredil, Technical datasheet, X MESH C10 RUREDIL X MESH C10 2013, pp. 1–6.
[50] M. Gold, F. Reinforced, C. Matrix, T. Ruredil, M. Gold, F. Ruredil, et al., Ruredil Ruredil X Mesh Gold, n.d.
[51] SIKA Technical datasheet, SikaWrap-350G Grid data sheet, 2016, n.d.
[52] U. Ebead, Inexpensive strengthening technique for partially loaded reinforced concrete beams: experimental study, J. Mater. Civ. Eng. 11 (2015) 4015002.